

Are Crustal Fault Zones viable geothermal resources? Insights from the Pontgibaud Fault in French Massif Central

Hugo Duwiquet^{1,2,3}, Laurent Arbaret¹, Mathieu Bellanger³, Laurent Guillou-Frottier^{1,2}, Michael J. Heap⁴.

¹ ISTO, UMR 7327, Université d'Orléans, CNRS, BRGM, 1A rue de la Férellerie, 45071, Orléans, France

² BRGM, 3 av. C. Guillemin, BP39009, 45060, Orléans, Cedex 2, France

³ TLS-Geothermics, 14bis chemin de l'Enguille, 31180, St Genies-Bellevue, France

⁴ Institut de Physique de Globe de Strasbourg, UMR 7516 CNRS, Université de Strasbourg/EOST, 5 rue René Descartes, 67084, Strasbourg cedex, France

hugo.duwiquet@gmail.com

Keywords: Permeability, porosity, high-temperature geothermal system, numerical modelling, Pontgibaud, French Massif Central.

ABSTRACT

Numerous recent studies indicate that crustal-scale fault zones represent efficient conduits for meteoric fluid to flow down to mid-crustal depths (Haines et al., 2016), in particular near the brittle-ductile transition where temperature are around 350–450°C (Violay et al., 2016). The present study aims to understand the potential of a new and novel type of geothermal system for high temperature and electricity production: the Crustal Fault Zones (CFZ). The geothermal potential estimation in a basement context requires combination of geological, geophysical and thermal data. The Pontgibaud fault zone (Puy-de-Dôme, French Massif Central) includes an intensive multivariate dataset.

1. STRUCTURES AND FAVOURABLE FEATURES FOR FLUID CIRCULATION IN THE "LA SIOULE" LICENCE

Since 2014, TLS-Geothermics, a French company involved in geothermal exploration (<http://www.tls-geothermics.fr/>), have been keen to demonstrate the viability of CFZ's as a play for economic power generation. The demonstration of the potential of CFZ's is underway at a site in the French Massif Central (FMC) using an exploration licence named "La Sioule". Several geological observations and geophysical data, some of which being detailed in Figure 1, represent good indicators for high temperature geothermal exploitation (temperatures > 150°C for a depth lower than 3,500 m).

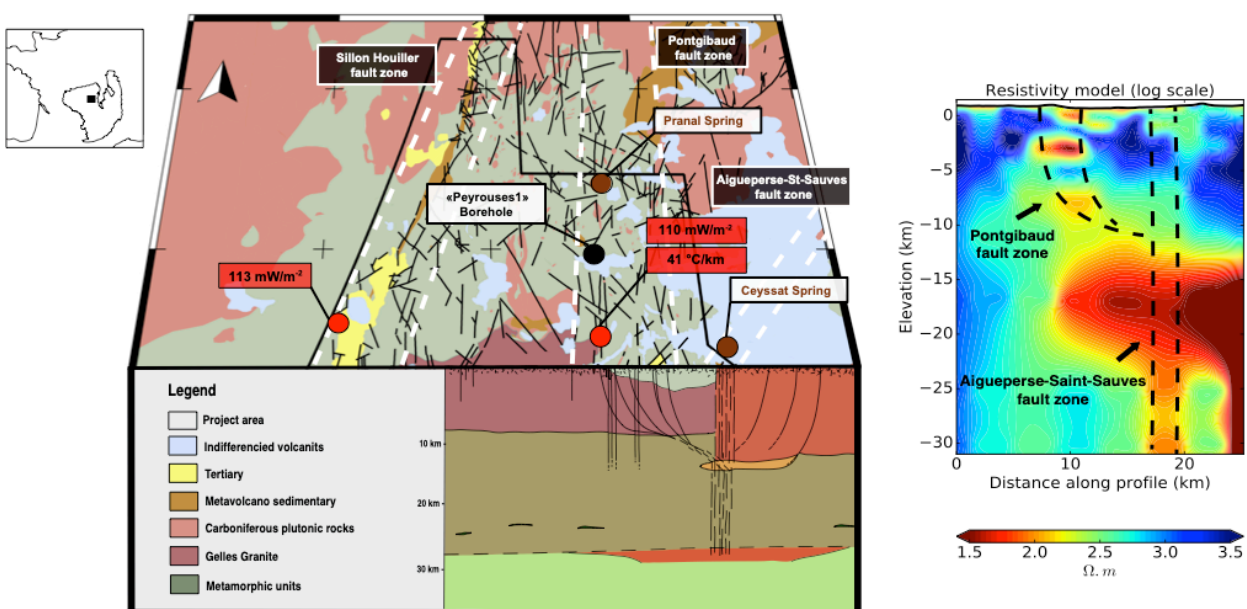


Figure 1 : Synthesis of critical available data on the "La Sioule" licence. Three principal fault zone are delineated by dashed white lines.

Magnetotelluric (MT) campaigns were carried out in the Pontgibaud fault zone area by TLS-Geothermics and IMAGIR (<http://www.imagir.eu/>) between 2015 and 2017 (Ars, 2018; Ars et al., 2019). From a 3D model of electrical resistivity produced in 2016 by IMAGIR, the profile corresponding to our geological cross-section was extracted (Fig. 1). This preliminary model has identified two electrical conductivity anomalies (Ars et al., 2017) The deeper one below 12 km depth could be related to the presence of fluids (hydrothermal fluids or silicate melt), which seems to be connected to the other low resistivity zone at 3 km depth (probably due to presence of smectite).

The Pontgibaud fault zone, of listric geometry, is associated with two other families of vertical faults. The presence of resurgences within these structures are indicators of fluid circulation. A micro-structural analysis of the samples collected within this hydrothermalized zone will help to understand how fluids flow within this deformed zone.

2. LABORATORY OBSERVATIONS AND ANALYSES

2.1 2D observations: thin-section

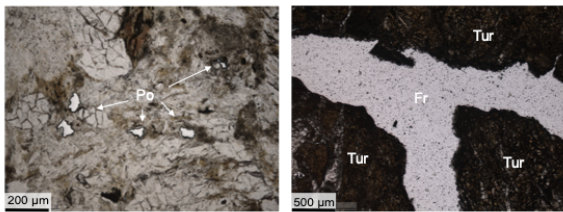


Figure 2 : Both observations of fracture (right) and matrix (left) porosity in thin-section. (Po) Porosity. (Fr) Fracture. (Tur) Turmaline.

Thin-sections observations (Fig 2) show highly altered facies (fractured anatexite, mineralized breccia and or porous breccia). These observations show that the fluid can circulate along the fracture and within the matrix in the fault zone. However, the only 2D observation does not show whether fluids can circulate throughout the system. To better understand this, 3D observations by X-ray micro-tomography were performed.

2.3 3D observations: X-ray microtomography

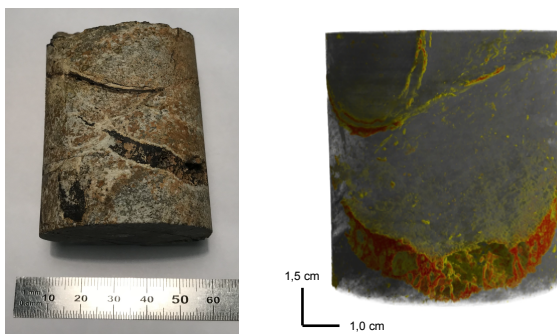


Figure 3 : Three-dimensional observations of samples comes from “Peyrouse 1 borehole”. Red color corresponds to mineralization (lead sulphides). The yellow colour correspond to the planar porosity located on the fracture walls (resolution of the figure is 25 µm).

X-ray micro-tomography is a non-destructive imaging technique that provides a three-dimensional visualisation of the analysed samples. This imaging technique makes it possible to obtain resolutions between 25 and 4 µm. This 3D visualization shows a high density of fractures; These fractures are distributed heterogeneously in space. This three-dimensional arrangement promotes connectivity of the pores located at the fracture walls (yellow in Fig 3). If the connectivity of planar porosity seems obvious, confirming the connectivity of matrix porosity is more delicate. Additional analyses with better resolution would allow a better visualization of their layout in three-dimensions.

Coupling thin-section (2D) and micro-tomography (3D) observations evidenced altered planar and matrix porosity filled by secondary minerals. Because this small-scale porous network can play a crucial role on fluid circulation within the Pontgibaud hydrothermal zone we performed direct measurements of connected porosity and permeability.

2.3 Laboratory measurement

Porosity and permeability properties were measured one the equipment available at the Ecole et Observatoire des Sciences de la Terre (EOST) in Strasbourg.

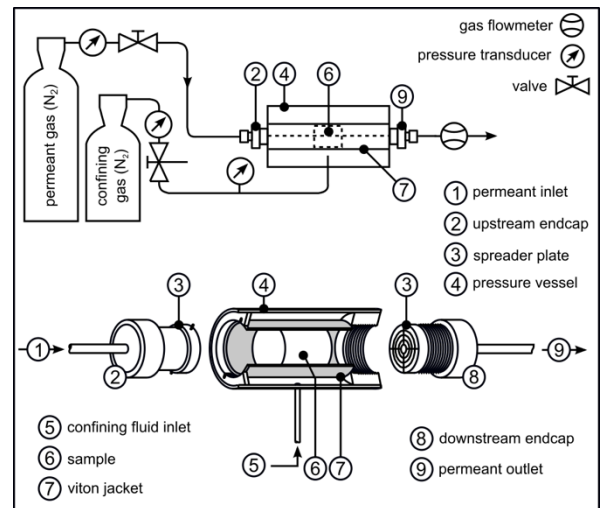


Figure 4 : Schematics of the experimental apparatus (from Heap & Kennedy, 2016)

These measurements were performed on the 7 samples for which the porosity was visualized by X-Ray micro-tomography. The followed experimental procedure is the one described by Heap & Kennedy (2016) (Fig 4). The permeability values vary between 2×10^{-18} and $7 \times 10^{-13} \text{ m}^2$ while the connected porosity values vary between 6 and 22% (Fig. 5). Overall, the highest is the permeability the highest is the connected porosity percentage, as illustrated by the two extreme values in figure 5.

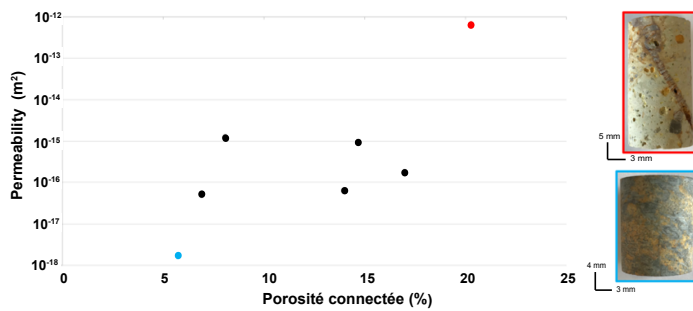


Figure 5 : Connected porosity and permeability measurements (according to the Heap & Kennedy (2016) method). In blue, sample 4-4-1 has a low degree of alteration. In red the sample 19-1-1 with a high degree of alteration. These purely qualitative degrees of alteration are based on macroscopic, microscopic observations and three-dimensional visualization by X-ray microtomography analysis.

To summarize, the three above-described results tend to suggest that fluids can circulate both in the matrix and in the pores. Hence, after having determined the first unknown parameter in section 1 (fault geometry), we identify here the second one (permeability variation). To better understand how fault geometry and permeability influence hydrothermal fluid flow and thus control the establishment of thermal anomalies, the numerical approach is required.

3. NUMERICAL APPROACH

3.1 Numerical procedure

The numerical simulation has been performed with Comsol Multiphysics™ software. In the numerical simulation we coupled the heat transfer and fluid flow equations with appropriate rock properties. For porous and permeable formations fluid motion is driven by pressure gradient and buoyancy, and fluid filtration velocity obeys Darcy's law.

3.2 Parametric study

More than 200 simulations were performed, with flat topography. The results of which are summarized in Figure 6. The images in Figure 6 represent temperature anomalies (ΔT), corresponding to the difference between temperature obtained in a conductive regime and the actual temperature as function of permeability and dip angle. The amplitude of the temperature anomalies are different for each case, and numerical values are indicated. In order to account for both the permeability of the fault and of the host rock, the R ratio (horizontal axis) compares the maximum permeability of the fault and of the basement (the permeability K_{b_0} being set at 10^{-16} m²). Other K_{b_0} values have been tested, but higher values are not realistic and lower values do not change the results detailed below.

As it can be seen in Figure 6, for $R = 200$, as the dip of the fault zone increases from 10 to 90°, the temperature values increase from 12 to 85.4°C (red numbers in Fig. 6). Thus, for a fixed R ratio, the highest thermal anomaly value will be for a vertical fault zone. The depth of the thermal anomaly also varies as a function of fault dip. By increasing the fault dip from 10 to 90°, the depth of the thermal anomaly (brown numbers in

Fig. 6) decreases from 3.6 to 0.7 km. Thus, for a fixed R value, vertical structures will result in the largest thermal anomalies at the shallowest depths.

By observing the variations in the temperature anomalies, we can see that when R increases for a fixed angle of 50°, the values of the thermal anomalies are 68.6, 82.5 and 77.4°C. Indeed, an increase in the R ratio does not show a significant increase in the temperature anomaly. However, the depth of these same anomalies decreases from 2.7 to 0.5 km. So for a fixed dip, when R ratio is high, the thermal anomaly will be at a maximum at a shallower depth. Therefore, a fault zone with a large dip and a high R ratio will result in the largest thermal anomalies at the shallowest depths. While this representation characterizes the distribution and intensity of positive thermal anomalies, it does not characterize the processes at their origin. The shape of the isotherms could reflect convection or conduction phenomena within the fault zone.

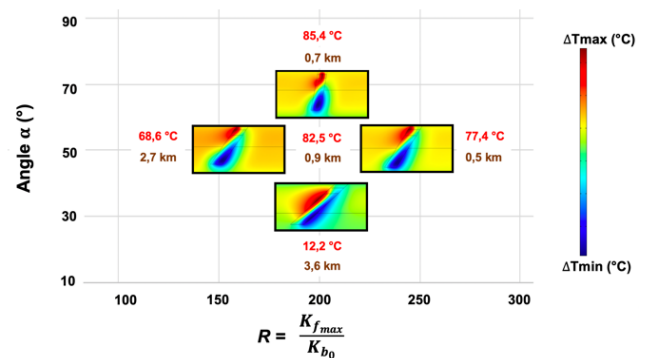


Figure 6 : Synthetic graphical representation of all the calculations performed. The values of positive thermal anomalies are shown in red. Their depths are shown in brown.

3.3 Comparison with the Pontgibaud natural system

Figure 7 presents the results of the numerical simulations with the temperature field (colors) and isotherms in white. In Figure 6a, the K_{f_0} imposed on the Pontgibaud fault zone ranges from 1×10^{-18} to 7×10^{-18} m². For these K_{f_0} values, the isotherms are not deformed, but are disturbed around the cooling magma chambers. At time $t_0 + 15,000$ years (Martel et al., 2013), the cooling of the magma chambers does not disturb any isotherms in the Pontgibaud fault zone. At this time step, nothing seems to disturb the position of isotherms within the Pontgibaud fault zone.

The deformed isotherms shown in Fig. 7b and 7c are located at the intersection between the Pontgibaud listric geometry and the vertical faults (see black box, Fig. 7a). For K_{f_0} values between 8×10^{-18} and 8×10^{-17} m², the deformation of the isotherms can be observed (Fig. 7b). This deformation increases from $K_{f_0} = 8 \times 10^{-18}$ m² to 8×10^{-17} m². This representation therefore shows that, when permeability is increased within the Pontgibaud fault zone, isotherms show an increasing disturbance.

Figure 7b shows the amplitudes and locations of the obtained thermal anomalies. These anomalies are represented as a function of R ratio, the value of the maximum temperature anomaly (ΔT_{max}) and its depth. As it can be seen in Figure 7b, positive and negative thermal anomalies are present in the Pontgibaud system. Positive thermal anomalies are located in the upper part of the fault zone, while negative thermal

anomalies are located at in the lower part of the fault zone.

4. COMBINING GEOPHYSICAL DATA AND NUMERICAL RESULTS

The Pontgibaud fault zone is defined by local and regional surface heat flow values of 110 mW.m^{-2} (International Heat Flow Commission database) involving temperature of 41°C/km . For fault zone permeability value of $8 \times 10^{-15} \text{ m}^2$, heat flux and geothermal gradient are respectively 115 mW.m^{-2} and 39°C/km . Furthermore, the overlaps of resistivity model and large-scale thermal anomaly map of Pontgibaud area (Figure 8) show a similitude between anomalously low resistivity zone and thermal anomalies. By keeping this overlapping result, we observed the establishment of a thermal anomaly of 150°C at 2,500 m.

5. CONCLUSION

The present study aims at investigating the possibility for the Pontgibaud crustal-scale fault zone to host an active hydrothermal system. Structural observations, laboratory permeability and connected porosity measurement and X-ray micro-tomography observations suggest that the hydrothermal system behaves like a double matrix-fracture permeability reservoir. Finally, numerical models of the geologically constrained Pontgibaud fault zone show that a temperature of 150°C at a depth of 2,500m can be obtained for a fault zone permeability of $8 \times 10^{-15} \text{ m}^2$. The resulting thermal regime down to 15 km depth appears consistent with previously obtained resistivity profiles. Based on multi-disciplinary approach, this work established a potential predictive tool for future high-temperature geothermal operations in a basement context. Nevertheless, additional petrophysical data and numerical models need to be performed in order to better constrain the understanding of the Pontgibaud hydrothermal system.

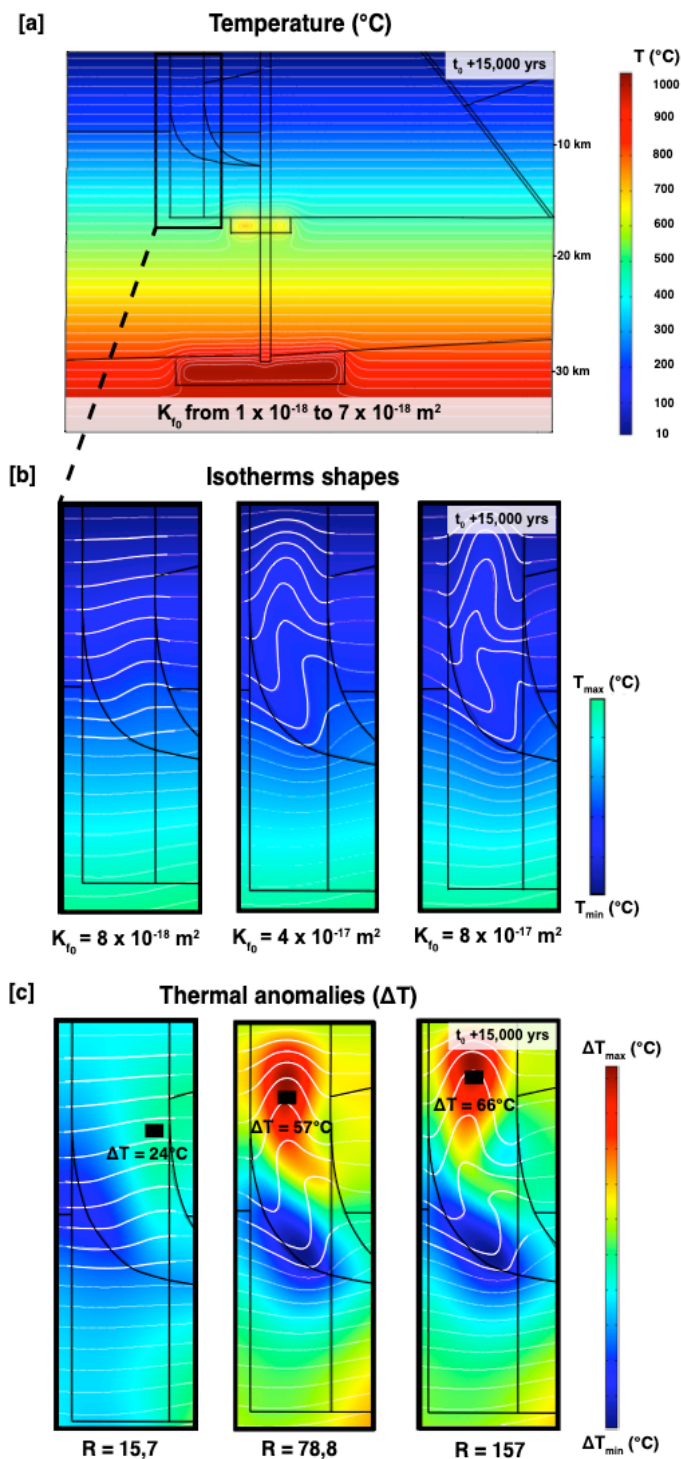


Figure 7 : Maps of crustal-scale temperature field [a] isotherms for three fault permeabilities [b], and thermal anomalies for three R ratios [c] of the Pontgibaud region.

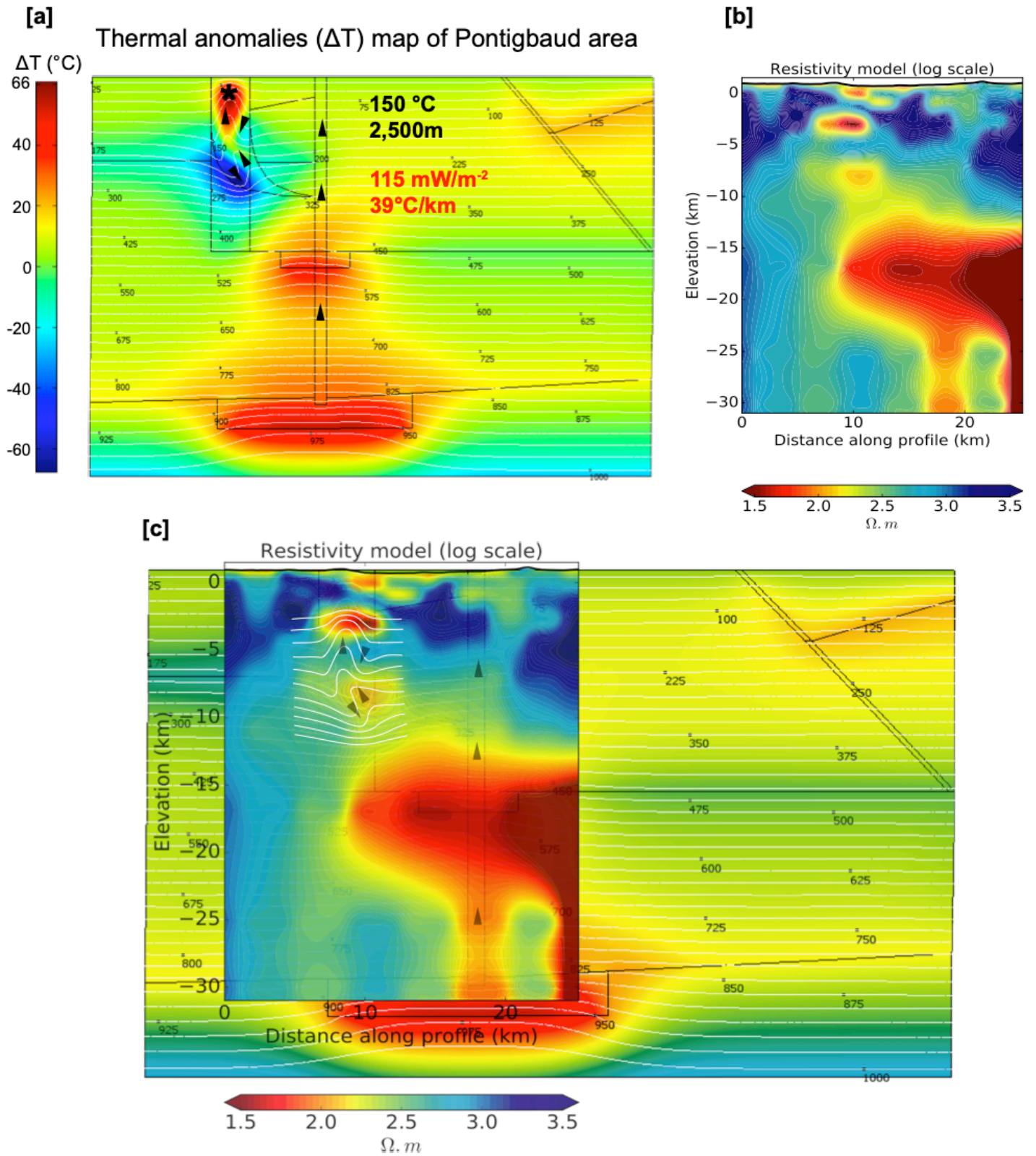


Figure 8 : Comparison between numerical simulations results and field data.

REFERENCES

- Ars, J-M.: (2018). Inversion conjointe géophysique appliquée à l'exploration en géothermie profonde dans le Massif Central. Thesis, University of Brest, (2018).
- Ars, J-M. Tarits, P. Hautot, S. Bellanger, M. Coutant, O. Maïa, M. : Joint inversion of gravity and surface wave data constrained by magnetotelluric: application to deep geothermal exploration of crustal fault zone in felsic basement. *Geothermics* (2019), 80, p56-68.
- Haines, S. Lynch, E. Mulch, A. Valley, J-W. van der Pluijm, B.: Meteoric fluid infiltration in crustal-scale normal fault systems as indicated by $\delta^{18}\text{O}$ and $\delta^2\text{H}$ geochemistry and $^{40}\text{Ar}/^{39}\text{Ar}$ dating of neofomed clays in brittle fault rocks. *Lithosphere*. (2016),587-600.
- Heap, M-J. Kennedy, B-M.: Exploring the scale-dependent permeability of fractured andesite. *Earth and Planetary Science Letters*, (2016),139-150.
- Martel, C. Champallier, R. Prouteau, G. Pichavant, M. Arbaret, L. Balcone-Boissard, H. & Scaillet, B. Trachyte phase relations and implication for magma storage conditions in the Chaîne des Puys (French Massif Central), *Journal of Petrology*. (2013),1071-1107.
- Violay, M. Heap, M-J. Acosta, M. Madonna, C.: Porosity evolution at the brittle-ductile transition in the continental crust: Implication for deep hydro-geothermal circulation. *Scientific reports*, (2017),7705.